 © 2019 Uspekhi Fizicheskikh Nauk, Russian Academy of Sciences

PHYSICS OF OUR DAYS PACS number: **13.15.+g**

Coherent elastic neutrino scattering on atomic nucleus: recently discovered type of low-energy neutrino interaction

D Yu Akimov, V A Belov, A I Bolozdynya, Yu V Efremenko, A M Konovalov, A V Kumpan, D G Rudik, V V Sosnovtsev, A V Khromov, A V Shakirov

DOI: https://doi.org/10.3367/UFNe.2018.05.038356

Contents

1. **Introduction** **166**
2. **Coherent elastic neutrino–nucleus scattering** **167**
3. **Neutrino sources** **168**
   3.1 Reactor; 3.2 Accelerator
4. **Review of detection methods and experiments** **169**
   4.1 Low-threshold gas detectors; 4.2 Semiconductor detectors; 4.3 Low-temperature bolometers; 4.4 CCD-based detectors; 4.5 Liquid noble-gas detectors
5. **COHERENT multidetector experiment: first observation of the effect** **173**
6. **Further investigations. RED-100 experiment** **176**
7. **Conclusions** **177**
   References **177**

Abstract. **We present recent results on the first experimental observation of the coherent elastic scattering of the neutrino on atomic nuclei and review other experiments related to the detection and investigation of this process.**

Keywords: neutrino interactions, coherent elastic neutrino–nucleus scattering, Standard Model, neutrino detectors

1. Introduction

To honor the 100th anniversary of the birth of B M Pontecorvo, *Physics Uspekhi* published a special issue in 2014 with articles related to neutrino research [1–6]. The 60th anniversary of the Joint Institute for Nuclear Research (JINR) was also marked in *Physics–Uspekhi* by a review of the same subject [7]. However, these papers did not consider the process of coherent elastic neutrino–nucleus scattering (CEνNS) predicted more than 40 years ago and recently discovered by the COHERENT collaboration, which includes the authors of this paper. The corresponding article [8] was published in *Science* in 2017 (online version, August 3; in print, September 15). Here, we introduce the readers to this important fundamental process and describe the latest techniques for its observation and further investigation. It is important to note that there are no reviews yet regarding CEνNS detection either in Russian or in the foreign literature.

D Yu Akimov (1, 2, *), **V A Belov** (1, 2), **A I Bolozdynya** (2, †), **Yu V Efremenko** (3), **A M Konovalov** (1, 2, 4, ‡), **A V Kumpan** (2), **D G Rudik** (1, 2), **V V Sosnovtsev** (2), **A V Khromov** (2), **A V Shakirov** (2)
(1) Alikhanov Institute for Theoretical and Experimental Physics, National Research Center "Kurchatov Institute", ul. Bol'shaya Cheremushkinskaya 25, 117218 Moscow, Russian Federation
(2) National Research Nuclear University MEPhI (Moscow Engineering Physics Institute), Kashirskoe shosse 31, 115409 Moscow, Russian Federation
(3) University of Tennessee, 1408 Circle Dr, Knoxville, TN 37996-1200, USA
(4) Moscow Institute of Physics and Technology (State University), Institutskii per. 9, 141700 Dolgoprudnyi, Moscow region, Russian Federation
E-mail: * akimov_d@itep.ru, † AIBolozdynya@mephi.ru, ‡ aleksei.konovalov@phystech.edu

Received 13 February 2018, revised 16 May 2018
Uspekhi Fizicheskikh Nauk **189** (2) 173 – 186 (2019)
DOI: https://doi.org/10.3367/UFNr.2018.05.038356
Translated by A L Chekhov; edited by A M Semikhatov

The CEνNS process is predicted and described in the framework of the Standard Model of fundamental interactions. The possibility of such a process was almost simultaneously considered for the first time by Russian [9] and American [10] scientists soon after the observation of the weak neutral current in neutrino interactions with the nuclei of a target [11]. The authors of these pioneering works noted that neutrinos and antineutrinos of all types can undergo coherent elastic interaction with all nucleons of the nucleus through a neutral current under the condition that only a small amount of the momentum is transferred to the nucleus. The cross section of such a process is relatively high: more than two orders of magnitude higher (for heavy nuclei) than the cross sections of other known interaction processes with high-energy neutrinos. CEνNS prevails when the neutrino interacts with atoms and plays an important role in the processes involving intensive neutrino fluxes in the Universe. As an example, we recall supernova explosions. During these processes, the kinetic energy of the outgoing neutrinos is almost 99% of the energy emitted during the explosion.

However, until recently there have been no experimental confirmations of the considered process due to great difficulties in detecting: the coherent elastic scattering of neutrinos with an energy of several dozen MeV on a heavy nucleus has an energy release of the order of a keV, while for nuclear reactor neutrinos with a mean energy of 2 MeV, the energy release is of the order of several hundred electron volts. In order to observe CEνNS, one needs a low-threshold detector with a large mass (more than several kilograms) operating in the low-background regime. CEνNS detection was considered not only another possibility of confirming the Standard Model but also a possibility of studying physics beyond this model.

An important stimulus for performing experiments to detect CEνNS is the possibility of using this scattering as a new tool for precise distant monitoring of nuclear reactors by the neutrino radiation. If elements with an atomic mass of the order of 100 and larger were used as an active medium in the detector, the interaction cross section would be several hundred times higher than the cross section of the inverse beta decay, which is traditionally used for the detection of reactor antineutrinos.

Progress in neutrino experimental physics requires a great effort, which is obviously due to the extremely low cross section of neutrino interactions. Therefore, every discovery in this field, on the one hand, is of large fundamental significance and, on the other hand, is a triumph of the detection technology used.

A significant part of this article is related to the first observation of the CEνNS process in an experiment performed by the COHERENT international collaboration at the Oak Ridge National Laboratory (USA). We also review experiments aimed at the detection and investigation of coherent elastic scattering of the neutrino on atomic nuclei in order to show the state of the art of research in this field. Finally, we consider the prospects of further investigations and applications of the CEνNS process.

2. Coherent elastic neutrino–nucleus scattering

The principle of coherence for neutrino scattering on an atomic nucleus is explained in [12] using a system consisting of A centers (in our case, nucleons) located at arbitrary points $\mathbf{x}_j$, $j = 1, 2, \ldots, A$, on which the elementary particle (neutrino) can scatter. The amplitude of the scattering on this system for a particle with a momentum $\mathbf{k}$ in the initial state and $\mathbf{k}'$ in the final state can be represented as a sum of the scattering amplitudes $f_j(\mathbf{k}', \mathbf{k})$ for each center with corresponding phase factors:

$$F(\mathbf{k}', \mathbf{k}) = \sum_{j=1}^{A} f_j(\mathbf{k}', \mathbf{k}) \exp\left[\mathrm{i}(\mathbf{k}' - \mathbf{k})\mathbf{x}_j\right]. \tag{1}$$

The differential cross section is proportional to the square of the amplitude and depends on the relation between the transmitted momentum $q = |\mathbf{k}' - \mathbf{k}|$ and the size R of the system ($R = \max_{i,j} |\mathbf{x}_i - \mathbf{x}_j|$). If the dimensionless value qR is of the order of unity or higher, then the individual scattering amplitudes strongly cancel each other, and the resulting cross section is small. If $qR \ll 1$, then the phase change on the scale of the system R is small. In this case, the amplitudes $f_j(\mathbf{k}', \mathbf{k})$ add constructively and the resulting cross section is proportional to $A^2 |\bar{f}(\mathbf{k}' - \mathbf{k})|^2$, where $\bar{f}(\mathbf{k}' - \mathbf{k})$ is the scattering amplitude averaged over the system.

For heavy nuclei, the condition $qR \ll 1$ is fulfilled for all scattering angles if the neutrino energy is not more than several MeV. For higher energies, the scattering is also coherent, but only for a specific range of small angles that allow the above condition to be satisfied.

According to the Standard Model, similarly to the elastic neutrino–proton scattering [13] and with the above ideas of coherence taken into account, the differential cross section of the CEνNS process is [14]

$$\frac{\mathrm{d}\sigma_{\mathrm{coh}}}{\mathrm{d}T} = \frac{G_{\mathrm{F}}^2 M}{2\pi} \left[(G_{\mathrm{V}} + G_{\mathrm{A}})^2 + (G_{\mathrm{V}} - G_{\mathrm{A}})^2 \times \left(1 - \frac{T}{E_\nu}\right)^2 - (G_{\mathrm{V}}^2 - G_{\mathrm{A}}^2) \frac{MT}{E_\nu^2} \right], \tag{2}$$

$$G_{\mathrm{V}} = (g_{\mathrm{V}}^{\mathrm{p}} Z + g_{\mathrm{V}}^{\mathrm{n}} N) F_{\mathrm{nucl}}^{\mathrm{V}}(Q^2), \tag{3}$$

$$G_{\mathrm{A}} = \left(g_{\mathrm{A}}^{\mathrm{p}}(Z_+ - Z_-) + g_{\mathrm{A}}^{\mathrm{n}}(N_+ - N_-)\right) F_{\mathrm{nucl}}^{\mathrm{A}}(Q^2), \tag{4}$$

where G_{F} is the Fermi constant, M is the nucleus mass, T is the nucleus recoil energy, E_ν is the neutrino energy, $g_{\mathrm{V}}^{\mathrm{n,p}}$ and $g_{\mathrm{A}}^{\mathrm{n,p}}$ are the vector and axial couplings of the Z boson with neutrons and protons, respectively, Z and N are the numbers of protons and neutrons in the nuclei, $Z_\pm$ and $N_\pm$ are the numbers of protons and neutrons with opposite spins, Q is the four-momentum transfer, and $F_{\mathrm{nucl}}^{\mathrm{V}}(Q^2)$ and $F_{\mathrm{nucl}}^{\mathrm{A}}(Q^2)$ are the vector and axial nuclear form factors, which are close to unity for small values of Q^2 ($|Q| R_{\mathrm{A}} \ll 1$, where R_{A} is the nucleus radius). The vector constants $g_{\mathrm{V}}^{\mathrm{n}}$ and $g_{\mathrm{V}}^{\mathrm{p}}$ are expressed as

$$g_{\mathrm{V}}^{\mathrm{p}} = \rho_{\nu\mathrm{N}}^{\mathrm{NC}} \left(\frac{1}{2} - 2\hat{\kappa}_{\nu\mathrm{N}} \sin^2\theta_{\mathrm{W}}\right) + 2\lambda^{\mathrm{uL}} + 2\lambda^{\mathrm{uR}} + \lambda^{\mathrm{dL}} + \lambda^{\mathrm{dR}}, \tag{5}$$

$$g_{\mathrm{V}}^{\mathrm{n}} = -\frac{1}{2}\rho_{\nu\mathrm{N}}^{\mathrm{NC}} + \lambda^{\mathrm{uL}} + \lambda^{\mathrm{uR}} + 2\lambda^{\mathrm{dL}} + 2\lambda^{\mathrm{dR}}, \tag{6}$$

where θ_{W} is the electroweak mixing angle and $\rho_{\nu\mathrm{N}}^{\mathrm{NC}} = 1.0086$, $\hat{\kappa}_{\nu\mathrm{N}} = 0.9978$, $\lambda^{\mathrm{uL}} = -0.0031$, $\lambda^{\mathrm{dL}} = -0.0025$, $\lambda^{\mathrm{dR}} = 2\lambda^{\mathrm{uR}} = 7.5 \times 10^{-5}$ are radiative corrections. For heavy nuclei, the axial contribution is small because it is determined only by unpaired protons and neutrons, the number of which is small in comparison with the total number of nucleons. Obviously, this contribution is zero for nuclei with zero spin. Hence, for the axial couplings of nucleons with the Z boson, we can use the values given in [13]:

$$g_{\mathrm{A}}^{\mathrm{p}} = 1.27/2, \qquad g_{\mathrm{A}}^{\mathrm{n}} = -1.27/2.$$

If we ignore the axial contribution, then, for $T \ll E_\nu$, we can write

$$\frac{\mathrm{d}\sigma_{\mathrm{coh}}}{\mathrm{d}T} = \frac{G_{\mathrm{F}}^2}{4\pi} M Q_{\mathrm{W}}^2 \left(1 - \frac{MT}{2E_\nu^2}\right) F_{\mathrm{nucl}}^2(Q^2), \tag{7}$$

where $Q_{\mathrm{W}} = \left[Z(1 - 4\sin^2\theta_{\mathrm{W}}) - N\right]$ is the weak nuclear charge. Because $\sin^2\theta_{\mathrm{W}} \approx 0.25$, it follows that $Q_{\mathrm{W}}^2 \approx N^2$ and $\mathrm{d}\sigma_{\mathrm{coh}}/\mathrm{d}T \sim N^2$. This means that the interaction probability (scattering cross section) significantly increases compared with the probability of interaction with single nucleons and scales as approximately the square of the number of neutrons in the nucleus. The total cross section can be estimated as

$$\sigma \approx 0.4 \times 10^{-44} N^2 (E_\nu)^2 \quad [\mathrm{cm}^2], \tag{8}$$

where N is the number of neutrons in the nucleus and E_ν is the neutrino energy in MeV [15].

Over the last several years, there has been great interest in models beyond the Standard Model [14, 16, 17]. As an example, we consider an additional interaction between the electron neutrino and quarks. $G_{\rm V}$ can be expressed as [14]

$$G_{\rm V} = \left[(g_{\rm V}^{\rm p} + 2\epsilon_{\rm ee}^{\rm uV} + \epsilon_{\rm ee}^{\rm dV})Z + (g_{\rm V}^{\rm n} + \epsilon_{\rm ee}^{\rm uV} + 2\epsilon_{\rm ee}^{\rm dV})N\right] F_{\rm nucl}^{\rm V}(Q^2)\,, \tag{9}$$

where $\epsilon_{\rm ee}^{\rm uV}$ and $\epsilon_{\rm ee}^{\rm dV}$ are the couplings with u and d quarks (we can describe the interaction of other types of neutrinos, ν_μ and ν_τ, similarly). This makes it interesting to measure the cross section of the interaction between the neutrino and the detector medium with an accuracy that would lead to a conclusion as to whether the Standard Model predictions are correct or this model has to be extended. The experimental sensitivity to cross section corrections of this kind can be significantly improved if detectors (simultaneously acting as targets) with different elemental compositions were used. Systematic errors related to the uncertainty in the definition of the neutrino beam intensity would then eliminate each other. It is also convenient to use targets with even–even nuclei, because the accuracy of the Standard Model prediction for them is the highest due to the absence of an axial contribution. The first estimate of the nonstandard interaction contribution [18] was reported almost immediately after the publication of the first observation of CEνNS by the COHERENT collaboration.

The measurement of the cross section for the elastic scattering of the neutrino on an atomic nucleus allows independently estimating the angle $\theta_{\rm W}$ at low energies. The angle $\theta_{\rm W}$ was measured with good accuracy in a number of experiments mainly for high energies (> 100 MeV, the Particle Data Group reports the value $\sin^2\theta_{\rm W} = 0.23120$ [19] measured at energies of about 100 GeV). The measurement of this value at low energies can also indicate the existence of new physics and, for example, explain the $(g-2)_\mu$ anomaly [20, 21].

If the neutrino has a large magnetic moment, which is also possible outside the Standard Model, then this property should reveal itself in CEνNS. The change in the shape of the low-energy spectrum of the recoil nuclei should provide bounds on the neutrino magnetic moment. In the framework of the Standard Model, the magnetic moment of a Dirac neutrino is expressed as [22]

$$\mu_\nu = \frac{3eG_{\rm F}\, m_\nu}{8\sqrt{2}\,\pi^2} \approx 3.2\times10^{-19}\left(\frac{m_\nu}{1\ {\rm eV}}\right)\mu_{\rm B}\,,$$

where $\mu_{\rm B}$ is the Bohr magneton. Current bounds on the electron neutrino magnetic moment were obtained from an analysis of $\nu_{\rm e}-{\rm e}$ scattering experiments and are of the order of $3\times10^{-11}\mu_{\rm B}$ [23, 24]. The shape of the energy spectrum of recoil nuclei in CEνNS is sensitive to somewhat larger values of the magnetic moment, of the order of several units of $10^{-10}\mu_{\rm B}$ [25], which is close to the bound for the muon neutrino obtained from the $\nu_\mu-{\rm e}$ scattering experiment [26]. However, it is important that this possible information can be obtained using another interaction channel.

Another quite exotic application of CEνNS is the measurement of the neutron distribution in the nucleus, i.e., the nuclear form factor [27, 28]. This is possible because the proton part of the nuclear weak charge is almost zero (the value of $\sin^2\theta_{\rm W}$ is close to 0.25) and the energy spectrum of the recoil nuclei gives information on the neutron component of the nuclear form factor. The first estimate of the neutron radius for Cs and I nucleons based on the energy spectrum of the recoil nuclei in the CsI[Na] crystal obtained by the COHERENT collaboration is given in [29].

3. Neutrino sources

3.1 Reactor

A 'classic' neutrino (electron antineutrino, to be precise) source is the reactor of a nuclear power plant (NPP). The thermal power of modern NPPs is more than 3 GW. Antineutrinos are emitted in β^- decays of fission fragments overloaded with neutrons. If we take into account that one fission event of nuclear fuel produces an energy of $\sim$ 200 MeV and emits around 6 antineutrinos on average, then the total antineutrino flux from a 3 GW reactor is $\sim 6\times10^{20}$ s^{-1}. Figure 1 [30] shows the antineutrino energy spectrum for various nuclear fuel components: ^{235}U, ^{239}Pu, ^{241}Pu, and ^{238}U. It is clear from the dependences that the antineutrino energy spectra are different for different components. The values of the mean energy release per decay vary as well. During the operation of a nuclear reactor, the relative composition of the fuel changes: the 'burning-out' of uranium is accompanied by the accumulation of plutonium, which undergoes fission as well. If the power of the reactor is maintained at a constant level, these factors lead to changes in the flux and the energy spectrum shape of the reactor antineutrino. This, in turn, allows nonintrusively monitoring the nuclear reactor using a neutrino detector [31, 32]. Reactors used as antineutrino sources in CEνNS experiments are reviewed in Table 2 in Section 4.

3.2 Accelerator

The collision of accelerated protons with a target can lead to the formation of stopped π^+ mesons, which are another source of neutrinos suitable for the investigation of the CEνNS process. An intense proton beam with a proton energy of the order of 1 GeV generates π^+ and π^- mesons when colliding with the target. The π^- mesons are quickly captured by the atomic nuclei, while the stopped π^+ mesons decay into monochromatic neutrinos ν_μ with the energy of 30 MeV and muons with the lifetime of 2.2 μs. These last emit $\bar\nu_\mu$ and $\nu_{\rm e}$ neutrinos with energies of the order of several

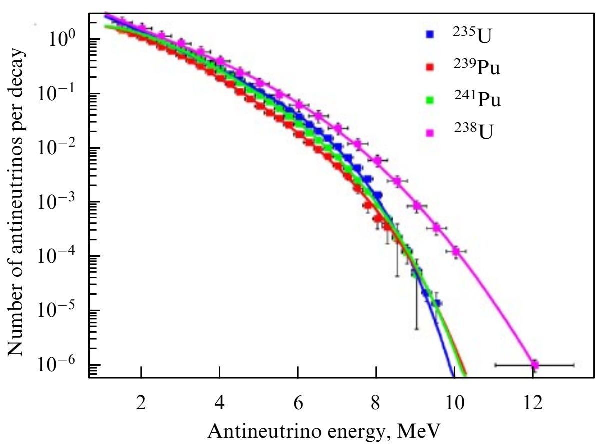

Figure 1. (Color online.) Energy spectrum of reactor antineutrinos for various components of the nuclear fuel. (Taken from [30].)

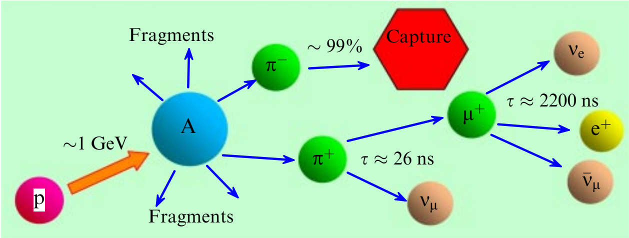

Figure 2. Neutrino production mechanism for the interaction of accelerated protons with a target. (Taken from [33].)

dozen MeV (Fig. 2) [33]. The contribution of neutrinos from in-flight decay of the π^+ mesons is not high, and hence the smearing of the lines of the 30 MeV muon neutrinos is very small. The time structure is as follows: muon neutrinos are generated exactly when the protons hit the target, while the majority of the electron neutrinos and muon antineutrinos form several microseconds after the collision, with the flux intensity decay constant being 2.2 μs, as defined by the muon lifetime. For a target power output of the order of 1 MW, the mean neutrino flux is several million times less than in the case of a nuclear reactor, while the interaction cross section is several hundred times larger due to the higher neutrino energy [the interaction cross section increases as the square of the neutrino energy according to Eqn (8)].

An important factor used for the suppression of background radiation unrelated to the accelerator operation is the pulsed time structure of the neutrino flux. In Table 1 (taken with some improvements from [34]), we compare the characteristics of planned and currently operating accelerator facilities that are sources of high-power neutrinos produced in π^+-meson decays. The best conditions are defined by the total intensity (power output on the target) and the background suppression factor determined by the ratio between the duration of the neutrino emission and the time interval between the collisions. Among the currently operating accelerator facilities, the best characteristics are obtained at the MLF (Japan Proton Accelerator Research Complex) and SNS (Oak Ridge National Laboratory).

The main task of the SNS accelerator complex is to produce high-intensity neutron beams for various applied tasks. The protons are sent to the target from rapidly circulating liquid mercury (with a speed of ≈ 300 kg s^{-1}). The duration of the proton beam is around 700 ns and the pulse repetition rate is 50 Hz, whence the time interval between the collisions is 16.7 ms. If we consider the observation time ~ 15 μs equal to the pulse duration plus several muon lifetimes, then the background suppression factor is approximately 1:1000. During a time interval corresponding to the collision of the protons with the target, one should observe a rapid 30 MeV ν_μ component from the π^+-meson decays, while the $\bar{\nu}_\mu$ and ν_e components should be observed as an exponential intensity decrease with a characteristic time of 2.2 μs due to muon decay. This temporal structure is an additional criterion for the extraction of the neutron signal in the detector.

4. Review of detection methods and experiments

The first paper discussing the possible realization of an experiment on CEνNS observation [15] was published a decade after the possibility of CEνNS had been reported [10]. The idea was to use a detector based on superconducting grains. This type of detector soon topped the list of devices for the search for hypothetical weakly interacting massive particles (WIMPs), the dark matter particles [35].

The operation of the detector was based on small (micrometer scale) metastable superconducting grains. The detector is placed inside a magnetic field and its temperature is set to such a value that even a very small energy release of the recoil nucleus after the neutrino scattering would lead to the loss of superconductivity in some of the grains. This leads to a measurable magnetic field variation, which should carry information about the energy released in the detector. Although this idea was not realized, it stimulated the development of a whole class of low-threshold low-background detectors to search for dark matter. In most cases, the developers of dark matter detectors also suggested using these detectors for the observation of CEνNS, because in both cases one needs to detect low-energy recoil nuclei (of the order of

Table 1. Characteristics of currently operating and planned neutrino sources based on the π^+-meson decay.

Accelerator facility	Location	Proton energy, GeV	Target power, MW	Bunch time structure	Repetition rate, Hz
LAMPF (Los Alamos Meson Physics Facility)	USA (Los Alamos National Laboratory)	0.8	0.8	600 μs	120
ISIS	Great Britain (Rutherford Appleton Laboratory)	0.8	0.16	2×200 ns	50
BNB (Booster Neutrino Beam)	USA (Fermi National Accelerator Laboratory)	8	0.032	1.6 μs	5–11
SNS (Spallation Neutron Source)	USA (Oak Ridge National Laboratory)	1	1.4	700 ns	60
MLF (Material and Life science experimental Facility)	Japan (J-PARC)	3	1	$2 \times (60-100)$ ns	25
CSNS (China Spallation Neutron Source)	China (planned)	1.6	0.1	< 500 ns	25
ESS (European Spallation Source)	Sweden (planned)	1.3	5	2 ms	17
DAEδALUS (Decay-At-rest Experiment for δ_{CP} studies At the Laboratory for Underground Science)	Planned	0.7	~ 7	100 ms	2

Table 2. Nuclear reactors used as antineutrino sources.

Reactor, NPP name	Location	Type	Reactor thermal power, MW	Experiment/ distance, m
San Onofre Nuclear Generating Station (SONGS)*	California (USA)	NPP	3000	CoGeNT/25
Kuo-Sheng	Wanli (Taiwan)	NPP	3000	TEXONO (Taiwan EXperiment On NeutrinO)/28
Kalinin NPP	Udomlya (Tver region, Russia)	NPP	3000	νGeN/10 – 12, RED-100**/19
Brokdorf	Brokdorf (Schleswig-Holstein, Germany)	NPP	3900	CONUS (COherent elastic NeUtrino nucleus Scattering)/17
Chooz	Chooz (Ardenne, France)	NPP	4300 × 2	Ricochet/355.4; 468.8
Massachusetts Institute of Technology Research Reactor (MITR)	Massachusetts Institute of Technology, Cambridge, USA	Research facility	5.5	Ricochet/7
Nuclear Science Center (NSC) Texas A&M University	Texas A&M University (USA)	Research facility (TRIGA***)	1	MINER (Mitchell Institute Neutrino Experiment at Reactor)/2
Angra	Angra dos Reis (Brazil)	NPP	4000	CONNIE (COherent Neutrino-Nucleus Interaction Experiment)/30

* Decommissioned.
** Planned. RED — Russian Emission Detector.
*** Training, Research, Isotopes, General Atomics.

10 keV or less for dark matter detectors and of the order of 1 keV or less for neutrino detectors). The experiments considered below and the reactors used in them are listed in Table 2.

We discuss known suggestions and experiments.

4.1 Low-threshold gas detectors

A large amount of attention was attracted to the detectors that use gas as the operating medium (target) scattering the neutrinos. These detectors allow strongly decreasing the energy threshold for the ionization signal detection due to, first, a significantly smaller recombination of the charge carriers with respect to that in denser liquid and solid media and, second, gas amplification, which provides an opportunity to register signals caused by single electrons. Theoretically, the threshold would be close to the mean energy needed to form a single electron–ion pair. However, the recoil nucleus transfers most of its kinetic energy to heat during collisions with other atoms, and therefore, for a heavy recoil nucleus, the mean electron–ion formation energy is much higher than that for electrons, for example.

In the late 1990s, the micro-mesh gaseous structure (MICROMEGAS) [36] and the gas electron multiplier (GEM) were demonstrated to support avalanche electron multiplication and were suggested as possible structures for the construction of gas detectors suitable for detecting the CEνNS process. A conventional gas proportional counter with cylindrical geometry was also suggested, with the amplification occurring on the central wire, the anode (see [38]).

The study mentioned above mainly discussed the signal detection methods with a low energy threshold. At the same time, important aspects such as the concepts underlying full-scale detectors, estimates of the background conditions, efficiency, and so on were not considered.

It is quite obvious that it is difficult to make a massive gas detector, which significantly limits its potential. This is the reason why there are not many proposals to use solely the gas detector.

4.2 Semiconductor detectors

The germanium detector with a 'point' contact opened a new era in low-background investigations. This detector has a low threshold because of the low equivalent noise due to the record-small value of the detector electrical capacitance. The energy threshold of such a detector is $\sim 0.2-0.3$ keV or even less.

The first collaborations to propose an experiment to observe CEνNS with detectors of this type were CoGeNT and TEXONO.

In the CoGeNT experiment [39, 40], the setup was placed at a distance of 25 meters from one of the reactors at the SONGS NPP (see Table 2) in a gallery where the ends of dome-reinforcing cables are fixed (tendon gallery). The equivalent thickness of concrete above the setup was approximately 30 meter water equivalent (m.w.e.). During the 2009 run, the background conditions were measured. It was shown that the detector energy threshold ~ 400 eV was too high for the registration of the CEνNS effect under the measured background level in the range of interest (~ 20 counts per keV $\times$ kg $\times$ day). After that, the experimental group switched to the search for dark matter, which does not need such a low energy threshold.

The TEXONO experiment [41] is being carried out at the neutrino laboratory of the Kuo-Sheng NPP in Taiwan. The setup is located at a distance of 28 m from the center of the reactor of the first power-generating unit. The collaboration currently has several low-threshold detectors with a 'point' contact (see [42]). It was shown that the energy threshold is of the order of 200 eV and, for lower energies, the registration efficiency gradually falls from 100% to zero at 100 eV. The collaboration has many tasks and among the main ones is the search for dark matter, on which the scientists are currently working.

Unlike the CoGeNT and TEXONO experiments, two other experiments with detectors of the same type, νGeN [43, 44] and CONUS [45], are dedicated to reactor antineutrino studies, and we may expect that they will deliver some results in the near future.[1]

The νGeN experiment is being conducted at the Kalinin NPP in a room located beneath power-generating unit 3 (WWER-1000 reactor, thermal power 3 GW; WWER is the water–water energy reactor). The concrete ceiling of the power-generating unit, the reactor itself, and the spent fuel storage pools located above this room form a shielding from the cosmic background with the overall equivalent thickness ≈ 70 m.w.e. The setup includes four germanium detectors, each weighing ≈ 400 g, which were developed and assembled in collaboration of JINR (Dubna) with BSI (Baltic Scientific Instruments) (Riga, Latvia). The detectors are installed in a common liquid-nitrogen-cooled cryostat placed in a multilayer passive shielding made of borated polyethylene, lead, and oxygen-free copper, combined with an active shielding of NaI(T1) right around the detectors and an active muon veto outside the passive shielding. All this, together with a thorough selection of material allowed reaching the background index of less than 1 count per keV $\times$ kg $\times$ day for the energy band below 1 keV. The threshold of the detectors is ~ 350 eV. A specific feature of the setup is that it is installed on a movable platform, which allows varying the distance to the reactor from 10 to 12 m. This gives additional information on the background, and the CEvNS effect can be extracted with higher accuracy.

The CONUS experiment is being carried out at the Brokdorf NPP (Germany). The thermal power of the reactor is 3.9 GW. The setup consists of four detectors with a total mass of 4 kg located inside a passive shielding made of lead and armored polyethylene combined with an active muon veto. The setup is located at a distance of ≈ 17 m from the center of the reactor core. The measured background is less than 1 count per keV $\times$ kg $\times$ day, but for the energy band 45–50 keV, which is quite far from the band of interest. There is no data on the energy threshold, but the signal amplitude is estimated for three threshold values: 0.18, 0.24, and 0.30 keV, which varies from several counts per day for the highest threshold to several dozen counts for the lowest one.

4.3 Low-temperature bolometers

In low-temperature bolometers, the energy release caused by a charged particle is measured by using the low-temperature effect of a very abrupt drop in the heat capacitance of the material with the temperature decrease. According to the Debye law, the dielectric heat capacitance can be expressed as

$$C = \lambda_{\mathrm{D}} \left(\frac{T}{\Theta_{\mathrm{D}}} \right)^3 , \qquad (10)$$

where $\lambda_{\mathrm{D}} = 1944\ \mathrm{J\ mol^{-1}\ K^{-1}}$, T is the temperature in Kelvin, and Θ_{D} is the Debye temperature. For Ge, for example, $\Theta_{\mathrm{D}} = 374$ K. At $T \sim 20$ mK (when Ge almost completely becomes dielectric), the heat capacitance is $C_{\mathrm{Ge}} \sim 1\ \mathrm{keV\ mol^{-1}\ \mu K^{-1}}$. This means that for a keV energy release, the temperature change ΔT is of the order of one millionth of a Kelvin and one would need special thermistors to detect it. For strongly ionizing particles, most of the deposited energy goes directly to heat, i.e., crystal lattice vibrations (phonons) in the case of a solid.

The Ricochet experiment [46] with low-temperature bolometers is planned at the Chooz NPP in France. There is an ongoing experiment, Double Chooz, at this power plant with detectors based on a liquid scintillator aimed at observing neutrino oscillations [47]. The authors of the experiment suggest using bolometers based on germanium and metallic zinc with the detector maximal total mass of 10 kg. It is suggested in [46] that the detector be placed inside the shielding of the 'closest' Double Chooz detector positioned at distances of 355.4 and 468.8 m from two reactors with a total power of 8.54 GW. The expected count rate of the detectors (5 kg Ge and 5 kg Zn) in the energy range from 0.1 to 1 keV should be approximately five counts per day for a background that is almost three times higher than the signal. Because such a count rate would not allow detailed studies of the CEνNS process, there are currently plans to locate the detector between the reactors (≈ 80 m from each reactor) [48]. There are also discussions about the CEνNS process detection near the Massachusetts Institute of Technology Research Reactor [49].

The MINER experiment [50, 51] is planned at the TRIGA Nuclear Science Center at Texas A&M University. The construction of the nuclear reactor allows placing the detector quite close to the reactor core (at a distance of approximately 2 m), which can be horizontally relocated inside a water tank. This will allow comparing measurements at different distances from the source with constant cosmic background conditions. It is planned to use low-temperature bolometers based on germanium and silicon that utilize the Neganov–Trofimov–Luke (NTL) effect for the amplification of the phonon signal (see [52] and the references therein), which will lead to a significant reduction in the energy threshold, down to ~ 10 eV. The estimated value of the count rate from the neutrino–detector interaction is 5 to 20 counts per keV $\times$ kg $\times$ day, depending on the distance to the reactor. Measurements of the neutrino and gamma background at the planned location have shown that in the energy range from 10 eV to 1 MeV, the background of a detector located at a distance of 2.3 m from the reactor core can reach a satisfactory value of approximately 100 counts per keV $\times$ kg $\times$ day, which should be enough to extract the neutrino–detector interaction signal.

Another recent project on CEνNS observation (announced before the results of the COHERENT collaboration were published) is the ν-cleus experiment [53]. This experiment is based on decreasing the energy threshold of a low-temperature bolometer to minimal values ~ 10 eV by decreasing the mass of the crystal. This is possible because the full width at half maximum of the energy resolution is determined by thermal fluctuations and is proportional to the square root of the crystal heat capacitance. The total mass of the setup should be increased by increasing the number of single crystals and merging them into layers. It is suggested to use $CaWO_4$ and Al_2O_3 crystals, implementing the technology developed in the well-known dark matter search experiment CRESST (Cryogenic Rare Event Search with Superconducting Thermometers).

[1] After this paper was accepted for publication, the CONUS group reported at the international conference Neutrino-2018 that the experimental data possibly include a CEνNS-related signal.

4.4 CCD-based detectors

An array of charge-coupled devices (CCDs) seems to be very promising for the detection of rare events with low energy deposition. Currently, this approach is used in the CONNIE experiment [54]. The detector is a stack of several 8-megapixel CCD arrays and actually operates as a track chamber. Events caused by interactions with neutrinos or, for example, dark matter WIMPs and neutrons appear in this detector as dots, i.e., are detected by individual cells of the array. At the same time, the interactions of charged particles — alpha particles, electrons (including those induced by gamma quanta), and muons — look like long tracks. This results in a very large suppression factor for the charged-particle background. Unfortunately, the mass of a single array used in the preliminary tests (approximately 5 g) is too small to detect the CEνNS process, even when measuring with multiple arrays. However, this project is of great interest because the implemented technology would be very promising if the detector mass is increased. The CONNIE collaboration is currently performing experiments at a test setup at the Angra NPP (Brazil). The setup is located at a distance of 40 m from the reactor core with a power of approximately 4 GW.

4.5 Liquid noble-gas detectors

The leading role in CEνNS investigations should be played by liquid noble-gas detectors, as has already happened in such a complicated experimental field as the search for WIMPs. The limit for the cross section of the spin-independent interaction between WIMPs and the detector medium rapidly began to improve in 2005 due to the appearance of emission detectors based on liquid xenon. This is mostly because such detectors can be scaled up quite easily: their dimensions can be increased without sectioning. This, together with three-dimensional (3D) coordinate sensitivity, gives the opportunity to locate some fiducial volume (FV) inside the detector, which would be well shielded from the external radioactivity by the active layer of the operating medium (the so-called concept of a wall-less detector [55]).

In the emission detector, which was suggested in the 1970s by Russian physicists [56], the main operating medium is the liquid phase of a noble gas, while the detecting part is the gas phase, to which the ionization tracks are pulled by an electric field. It is convenient to apply various well-proven methods for charge detection in gases. Such a detector is a sort of a time-projection chamber filled with liquid noble gas, in which the coordinate along the charge drift (vertical) is deduced from the drift time, while the scintillation signal gives the initial point. The location of the event in the horizontal plane is determined using a position-sensitive detector placed inside the gas phase (usually, a photomultiplier array registering the electroluminescence signal, also known as proportional scintillation).

4.5.1 Liquid argon. Although much effort was spent on the development of liquid-xenon dark matter detectors in the early 2000s, the authors of the first proposal for the CEνNS experiment [57] considered using a two-phase liquid-argon emission detector. Although the cross section of the interaction between the neutrino and the argon nucleus is much smaller, it seems that there was a specific reason for this choice. Because the argon nucleus has a smaller mass, the recoil nucleus has the kinetic energy approximately three times higher than in liquid xenon, and is easier to detect.

Thorough investigations of the two-phase argon emission detector were performed in a small test chamber at the Livermore National Laboratory (USA) [58]. Using this chamber and a radioactive isotope ^{37}Ar (K- and L-capture, 2.82 and 0.27 keV, respectively) contained in the detector's operating medium, the authors for the first time demonstrated the operation of the two-phase argon detector in the keV energy range and for energies less than 1 keV e.e. (electron equivalent) [59]. Another important achievement for the liquid-argon detector was the first measurement of the specific ionization yield for recoil nuclei with the kinetic energy of 6.7 keV [60]. It was shown that its value is in the range from 3.6 to 6.3 electrons per keV for an electric field strength from 0.24 to 2.13 kV cm^{-1}. This result demonstrated the fundamental possibility of detecting the CEνNS process using a liquid-argon detector. A two-phase liquid-argon emission detector is also being developed in Russia at the Budker Institute of Nuclear Physics (BINP), Siberian Branch of the Russian Academy of Sciences (Novosibirsk), to search for dark matter and to detect CEνNS [61].

Liquid argon also has a very important feature for particle detection: different types of particles can be efficiently separated by analyzing the shape of the scintillation signal in both single-phase and two-phase detectors. This is possible due to a very large difference between the lifetimes of the singlet and triplet states and hence between the de-excitation times of the fast ($\sim$ 7 ns) and the slow ($\sim$ 1600 ns) components [62]. The ratio between the values of the fast and slow components is larger for recoil nuclei than for recoil electrons. Such a difference between the de-excitation times is excessive for the particle separation method based on pulse shape analysis. If the value of the slow component were decreased to several hundred nanoseconds, it would give the following advantages: a general decrease in the background related to 'tails' from large preceding signals and the existence of a more compact slow part of the signal in the case of small energy release (when the slow component is represented by single photoelectrons that do not overlap in time). Several scientific groups are currently studying the possibility of decreasing the duration of the scintillation signal of liquid argon by adding a small amount of xenon to it (several dozen parts per million) [63, 64]. Unfortunately, natural argon has a quite high radioactivity ($\approx$ 5 mBq keV^{-1} kg^{-1}) [57] due to the beta decay of the cosmogenic isotope ^{39}Ar, which results in a background that is significantly higher than the count rate related to the CEνNS process, even if the detector is located close to the nuclear reactor. This beta background cannot be rejected in the experiment with reactor antineutrinos because the scintillation signal for the characteristic energy release is too low, of the order of single photoelectrons. Nevertheless, this method can be successfully applied for the detection of neutrinos produced by pion decay in accelerator experiments (see above) with a significantly higher energy release.

The first proposal for CEνNS process detection at the SNS accelerator was made in [65]. It was planned to place a detector based on liquid argon (LAr) or liquid neon (LNe) at a distance of 46 m from the target. The detector, with an active mass of 456 (391) kg of LAr (LNe), was proposed to be placed in a tank 24 feet (7.3 m) in diameter and 16 feet (4.9 m) in height filled with water and viewed with photomultiplier tubes (PMTs) — an active and passive veto. The active part of the detector was to be monitored using two arrays of PMTs (19 PMTs in each) with photocathodes coated with tetraphenyl-butadiene, which re-emits scintillation light into the visible range at wavelengths of 125 nm for LAr and 80 nm for LNe. For a total data taking time of 2.4×10^7 s per year with the SNS accelerator power of 1.4 MW, the LAr (LNe) CEνNS signal was expected to be of the order of 890 (340) events per year for the slow neutrino component and 210 (110) events per year for the fast one, with the energy threshold assumed to be 20 (30) keV. The radioactive background includes the neutron component and a large contribution from beta-active ^{39}Ar, which is suppressed by several orders of magnitude using signal selection by the pulse shape, and its total level is expected to be much lower than the CEνNS signal.

The CENNS-10 liquid-argon detector with an active mass of 22 kg is currently operating at the SNS [66]. The detector performs beta-particle background rejection by analyzing the pulse shape. CENNS-10 was built as a prototype for the CENNS project for observing CEνNS at the Fermi National Accelerator Laboratory (USA) [67].

4.5.2 Liquid xenon. Reports on the identification of single ionization electron signals in the two-phase xenon emission detector [68, 69] led to new proposals to use this type of apparatus to detect CEνNS [70, 71]. At that time, there was no experimental data on the specific ionization yield (the number of ionization electrons per keV) for the recoil nuclei in liquid xenon in the keV and sub-keV energy ranges. However, experiments have shown that as the recoil nuclei energy decreases and reaches this energy range, the specific ionization yield increases (see, e.g., [72]), which was very encouraging. Such a behavior of the specific ionization yield with an ionization density increase turned out to be very surprising because the semiconductor detectors demonstrated the opposite trend when registering the ionization signal. This effect was explained by the box model [73] put forth for the thermalization and recombination of electrons with ions in a liquid noble gas after their creation by a charged particle. The idea is as follows: as the energy of the ionizing charged particle decreases, the length of its track at some point becomes less than the characteristic thermalization length of the electrons formed during the ionization. Because only thermalized electrons can recombine with ions and the ion cloud cannot spread out within the thermalization time, the fraction of recombined electron–ion pairs decreases as the track length and the particle energy decrease. For higher energies, when the particle track is longer than the electron thermalization length, the 'classical' Birks regime takes place, and the specific yield decreases together with the energy due to the increase in the ionization density, which leads to an increase in the electron–ion recombination rate. This mechanism works for both liquid xenon and liquid argon, as well as for different types of particles: electrons and recoil nuclei. In the latter case, the increase in the specific ionization yield with the energy decrease is observed for higher recoil nuclei energies due to a different characteristic track length.

The physics of charged-particle interaction with liquid noble gases has been quite well studied and is implemented into the NEST package (Noble Element Simulation Technique) [74] (see also NEST the web page [75]), which models the scintillation and ionization response of a liquid noble gas for recoil nuclei and electrons (gamma quanta) with different energies.

The two-phase liquid-xenon emission detector (see Section 6 about the second-generation detector RED-100) is promising for CEνNS investigations due to the following most important advantages:

— as an operating medium, liquid xenon is one of the heaviest elements used in detectors. This gives the potential to obtain maximal values of the interaction cross section and at the same time reach the low energy threshold (~ 0.3 keV);

— allowing the registration of ultralow ionization signals down to single electrons and performing spectrometry, i.e., obtaining the signal strength distribution as separate peaks (if the light collection is efficient enough) corresponding to one, two, three, etc. ionization electrons in the signal;

— no long-lived radioactive isotopes in liquid xenon;

— high density and large Z of liquid xenon, which allows using the upper layer as efficient active and passive shielding.

5. COHERENT multidetector experiment: first observation of the effect

The international COHERENT collaboration was formed in 2014 with the goal to experimentally detect and investigate the CEνNS effect. The experiment is being performed at the SNS accelerator facility. The strategy is to use several detectors of different types, with various elemental compositions, in order to confirm the dependence $\sigma \sim N^2$. In the initial proposal published in [76], we considered three detector subsystems: a CsI[Na]-based detector, a two-phase liquid-xenon emission detector, and a germanium 'point' contact detector. In the final configuration [66], the xenon detector is replaced with the CENNS-10 single-phase liquid-argon detector. The detectors are installed in the basement of the target unit of the accelerator or, as the collaboration members have named this room, 'neutrino alley'. The basement is located at a depth corresponding to ≈ 8 m.w.e. at a minimal distance from the target (around 19 m). The detector arrangement is shown in Fig. 3 [66]. The distances between the detectors and the target are as follows: 28.4 m for the liquid-argon detector (CENNS-10), 21.1 m for the germanium detector (planned), and 19.3 m for the CsI[Na] detector. Besides the mentioned detectors, there are also other detectors installed in the 'alley': a NaI detector, which is currently being prepared to launch with the connection of some add-on modules (its current mass is 185 kg), the Neutron Scatter Camera, Scibath, and Multiplicity And Recoil Spectrometer (MARS) detectors based on a liquid scintillator for the study of the neutrino background, and NIN Cube detectors for the investigation of the neutron production reactions induced by the neutrino–medium

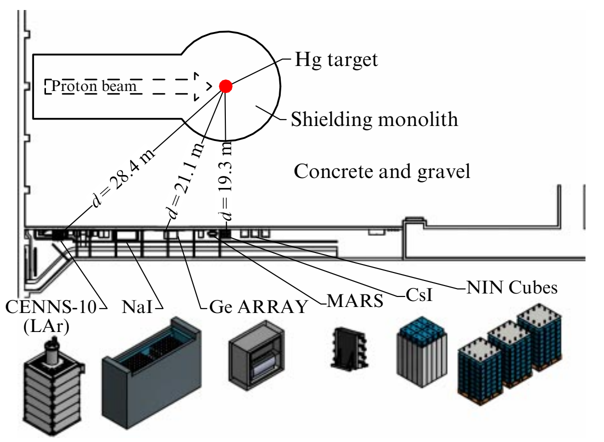

Figure 3. Arrangement of the detectors in the 'neutrino alley' at the SNS accelerator. (From [66].)

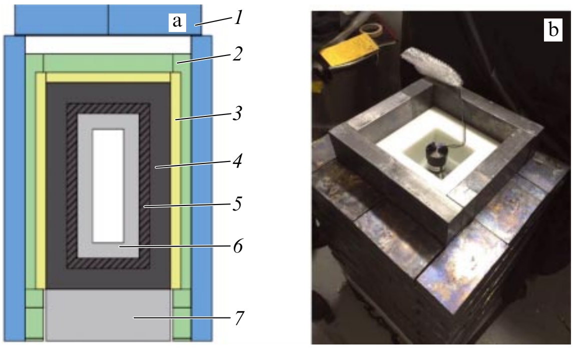

Figure 4. (a) Schematic and (b) general view of the radiation shield of the CsI detector at SNS [78, 79]: *1* — water, *2* — aluminum frame, *3* — muon veto, *4* — lead, *5* — low-radioactivity lead, *6,7* — high-density polyethylene, inner layer and base.

interaction (Neutrino Induced Neutrons, NINs). The last experiment is very important for estimating the neutron background contribution corresponding to neutrons that form after the neutrino interaction inside the neutron shielding of the detector.

The first observation of CEνNS was made using the CsI detector. We note that this was actually achieved not due to progress in particle detection technology (the experiment was performed using a conventional scintillation detector) but due to a good choice of the neutrino source and the detector location. The setup is located in the basement with a thick layer of ground shielding from neutrons emitted by the target, strongly reducing the neutron component of cosmic rays. The experimental results were based on the dataset accumulated in a 15-month period. The experiment is currently ongoing in order to increase the statistical accuracy.

The CsI detector (preliminary version) was described in detail in [77]. The final version of the setup is improved with an inner layer of high-density polyethylene with a thickness of 7.5 cm directly around the detector (*6* in Fig. 4). This additional layer should suppress the NIN background by more than one order of magnitude. This layer is followed by a layer (*5*) of special low-radioactivity lead with isotope contamination ^{210}Pb ~ 10 Bq kg^{-1} and 5 cm thickness, which is surrounded by a 10 cm layer of regular lead (*4*). This passive shielding is covered from above and from the sides with a scintillation veto detector (*3*) 5 cm in thickness with a 99.6% efficiency. Finally, the setup is surrounded by a neutron moderator: below, a 15 cm layer of high-density polyethylene (*7*), which is the base of the setup, and from above and from the sides, 9 cm thick tanks filled with water (*1*). The CsI[Na] crystal is grown from a specially selected low-radioactivity material by the Amcrys company (Institute for Single Crystals of the National Academy of Sciences of Ukraine) (Kharkiv). Having a mass of 14.57 kg, a height of 34 cm, and a diameter of 11 cm, it is monitored by one low-background PMT Hamamatsu R877-100 with high quantum efficiency (super bialkali photocathode).

This type of the detector was chosen due to the combination of several parameters. The sodium-doped CsI crystal contains heavy atomic nuclei of cesium and iodine, which have approximately equal masses and neutron numbers (74 and 78), which greatly simplifies the analysis of the experimental data. Among the detecting properties, we note, first, a high light yield of approximately 45 photons per keV e.e. in the spectral range that perfectly coincides with the spectral characteristic of the bialkali photocathode and, second, a shorter de-excitation time compared to that of CsI[T1]. The latter property is very important for measurements of low scintillation signals on top of the tails from large signals formed by a significant external background (mostly cosmic muons).

The most important characteristic of the scintillation detector as regards measuring the energy release caused by the heavy recoil nucleus is the so-called quenching factor (QF) — a quantity indicating what part of the released energy is transferred into light energy. For gamma quanta or electrons, its value is close to unity. Therefore, when calibrating the detector for recoil nuclei registration using the gamma quanta, the electron equivalent scale (keV e.e.) is used.

The QF was measured for a crystal with a smaller volume (22 cm^3) made by the same manufacturer and grown using the identical technology. The measurements were performed using a monochromatic neutron beam with an energy of 3.8 ± 0.2 MeV at the Triangle Universities Nuclear Laboratory (TUNL) [80]. The recoil nucleus energy in the elastic neutron–nucleus scattering was controlled with the neutron scattering angle, which was determined using a system of neutron counters located at various angles. Two independent series of measurements were performed using the same crystal for different geometries of the scattered neutron separation and different data analysis. This resulted in two slightly different QF values, which were averaged, while the difference was attributed to the uncertainty in the value (QF $= 8.78 \pm 1.66\%$).

The setup signals (from the CsI crystal and the total signal from all the panels of the scintillation veto) were digitalized using a two-channel analog-to-digital converter (ADC) NI-5153 with a 500 MHz sampling rate. The digitalization period was synchronized with a trigger corresponding to the instant of the proton collision with the SNS target. The data-recording window was 70 μs and the trigger position was 55 μs after the beginning of the window. The region close to the trigger was separated into two 12 μs windows before and after the trigger, in which the signals were analyzed in an identical way by integrating over the 3 μs window starting with the beginning of the signal. The neutrino signal can be observed only in the second 12 μs window, called the 'coincidence window'. The first window ('anticoincidence window') was used for the background measurement. Before each of these windows, broader 40 μs 'pre-trace' windows were set in order to detect the appearance of 'tails' from the preceding signals with large energy release. The pulses were not analyzed if the number of PMT pulses in the pre-trace exceeded the threshold value (except for overlapping events, each pulse corresponds to a single photoelectron). Approximately 25% of the traces were excluded due to this criterion.

Some other events were excluded due to 'quality' conditions: events coinciding in time with the muon veto signals, events blocked by a linear gate preventing PMT saturation, and signals higher than the ADC voltage range. When analyzing the signals detected in the coincidence and anticoincidence windows, there was an additional threshold for the number of PMT pulses in the integration interval of the considered window. The efficiency of such a threshold with respect to the expected signal was obtained using the calibration data. Two threshold values — for the number of PMT pulses in the pre-trace window and in the coincidence or

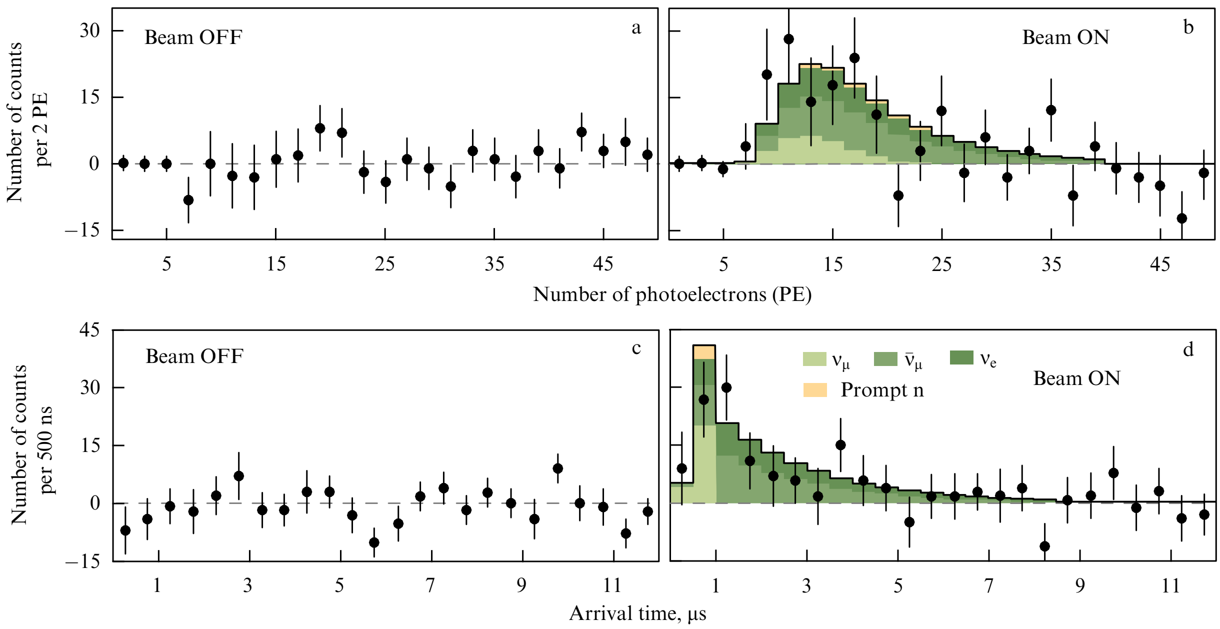

Figure 5. (Color online.) (a, b) Residual amplitude and (c, d) arrival time distributions for the neutrino interaction events in the CsI detector for the accelerator beam off (a, c) and on (b, d) (results of the analysis performed by the Russian group of the COHERENT collaboration); the histogram is the Standard Model prediction.

anticoincidence windows — were determined by optimizing the ratio of the expected CEνNS signal to the observed background counts in the anticoincidence window with the efficiency of the thresholds taken into account. The values of the thresholds are given in [8]: 3 pulses maximum for the pretrace window and 8 pulses minimum in the analyzed window (coincidence or anticoincidence). The last of these values determines the detector threshold with respect to the recoil nucleus energy, being approximately 7 keV.

The analysis of the signals selected using the above limitations in the coincidence and anticoincidence windows allowed obtaining the spectra of the signal values (integrals of the recorded signals over 3 μs intervals) and the time distribution of the signals for both periods of time: during the proton spills to the target and when the accelerator was off. Further analysis resulted in the residual spectra shown in Fig. 5 for each of the observed values: spectra corresponding to the anticoincidence window were subtracted from the ones corresponding to the coincidence window. This procedure excluded the contribution from a constant background (with no specific temporal structure). The obtained residual distributions included the CEνNS signal from the detector material and the contribution from the background processes that correlate with the proton spill on the accelerator target. Among the latter ones, the most dangerous are the 'direct' neutron background (neutrons formed during the interaction of protons with the target) and the NINs mentioned above.

The measurement of the neutron background is a quite complicated task if its level is very low. For this purpose, before the start of the measurements, the shielding of the CsI[Na] detector was equipped with two detectors based on the EJ-301 liquid scintillator, each 1.5 l in volume. The detectors could separate the neutron signals by the pulse shape. The inner layer of lead 2.5 cm in thickness and polyethylene were removed and the detectors acquired statistics over 170 days of the accelerator operation. The obtained energy spectrum of recoil nuclei was fitted in the range from 30 to 300 keV in order to obtain the total flux and spectrum of the neutron background outside the shielding. It was also assumed that the energy spectrum has a polynomial shape. This assumption is supported by the data from the Scibath liquid scintillator detector [81] and the neutron Scatter Camera [82], which measured the neutron background in different parts of the 'neutrino alley'. The sensitivity of these detectors allowed estimating the neutron flux in the energy range 1–100 MeV close to the location of the CsI[Na] shielding by a value of the order of 1.5×10^{-7} cm^{-2} s^{-1}. Part of the fitting procedure of the recoil nuclei spectra from the EJ-301 scintillator involved the modeling of the specific neutron flux propagation through the shielding and recoil nuclei generation, which was performed using the MCNP-X-PoLiMi program package [83]. This procedure resulted in estimating the neutron flux outside the shielding as 1.09×10^{-7} cm^{-2} s^{-1}, and the exponent of the spectrum was -1.6. Modeling the neutron background inside the shielding in the operating configuration (see Fig. 4) with the obtained neutron spectrum outside the shielding taken into account has shown that the neutron background contribution is approximately 25 times less than the expected CEνNS signal.

The possible NIN contribution can be estimated by using the distribution of the signal arrival times at the EJ-301 detectors with respect to the moment of proton–target collision. The main source of this background is the ^{208}Pb $(\nu_e, e^- xn)$ reaction [84, 85] involving the 'slow' component of the SNS neutrino flux. The characteristic time profile of the formation of 'decay' ν_e allows separating the NIN contribution from the flux of 'direct' neutrons. By fitting the time distribution obtained using the EJ-301 detector, it can be concluded that the NIN contribution is much (~ 47 times) lower than the expected signal caused by the CEνNS effect.

It is clear from the residual spectra shown in Fig. 5 [8] that for the periods of time when the accelerator was on, there are excesses both in the signal amplitude spectra and in the time distribution, which is in agreement with the expected contribution from CEνNS on the atomic nuclei of the detector material. At the same time, there are no excesses in the residual spectra that correspond to periods when the accelerator was off. To determine the significance of the observed effect, we used the fitting procedure for two-dimensional experimental distributions (over the amplitude and the arrival time of the signals) with contributions from 'direct' neutrons and the constant background taken into account. The resulting statistical significance of the CEνNS process observation is 6.7 σ. The total number of the registered events corresponding to the maximal value of the likelihood function was 134 ± 22, while the Standard Model prediction is 173 ± 48 events.

The main contribution to the prediction uncertainty comes from the uncertainty in the QF measurement for CsI[Na] ($\sim 25\%$). Moreover, a significant contribution comes from the uncertainties in the neutrino flux from SNS ($\sim 10\%$), the nuclear form factor ($\sim 5\%$), and the efficiency of the thresholds used in the analysis ($\sim 5\%$). This means that the overall accuracy of the prediction is currently 28%.

The COHERENT experiment continues to acquire statistics with the CsI[Na] detector. This, together with the planned additional measurement of the crystal QF, gives hope that the statistical accuracy of the number of observed events will soon increase and the uncertainty in the predicted value for the effect will decrease.

6. Further investigations. RED-100 experiment

After the first observation of the CEνNS process, it became obvious that investigations would continue using more sensitive detectors and in the lower energy range characteristic of the reactor antineutrinos. This range is the most complicated one, but on the other hand, the most interesting from the scientific and practical standpoints (neutrino monitoring of nuclear reactors). In Section 4, we reviewed those experiments where the reactor is mostly used as the neutrino source. Because the task to perform the first observation of this process is not of interest anymore, we turn to large-mass detectors, which can perform detailed studies with large statistical significance.

The two-phase liquid-xenon emission detector RED-100 (Fig. 6) belongs to this class of detectors and is ready to be installed near a nuclear reactor [86]. The operating medium (xenon) is maintained in the liquid state using a vacuum titanium cryostat (*1*, *2*). An electrode system is placed inside the cryostat to apply a uniform electric field to the liquid xenon, which is contained in a volume ≈ 380 mm in diameter and ≈ 410 mm high. This volume is surroundeded from above with an emission electrode (*5*), from the side with field-shaping rings (*7*), and from the bottom with a cathode (*9*). The anode (*4*) is located 19 mm higher than the emission electrode. The liquid-xenon surface level is maintained at the same distance from the electrode and the anode. The voltage between the anode and the emission electrode is ≈ 11 kV in order to provide an electric field strength ≈ 8 kV cm^{-1} in the gas phase. The cathode high-voltage supply system is designed for the maximal value ~ 40 kV, which corresponds to the electric field strength about 1 kV cm^{-1} in the drift region.

The anode, the emission electrode, and the cathode are flat meshes with hexagonal cells (with the optical transmission coefficient ≈ 0.83), fabricated from stainless steel foil using the electrolytical technique. The liquid-xenon volume is viewed by top (*3*) and bottom (*10*) PMT arrays (19 PMTs each) through these meshes. There are additional grounded hexagonal meshes in front of the PMT windows in order to minimize the electrostatic influence of the anode and cathode electrodes on the PMT operation. R11410-20 PMTs were developed by the Hamamatsu company (Japan) specifically for low-background detectors based on liquid xenon. These PMTs are designed for operation at cryogenic temperatures ($-100\,^{\circ}$C) and are sensitive to liquid-xenon luminescent light in the vacuum ultraviolet range (175 nm) with a quantum efficiency of about 30%.

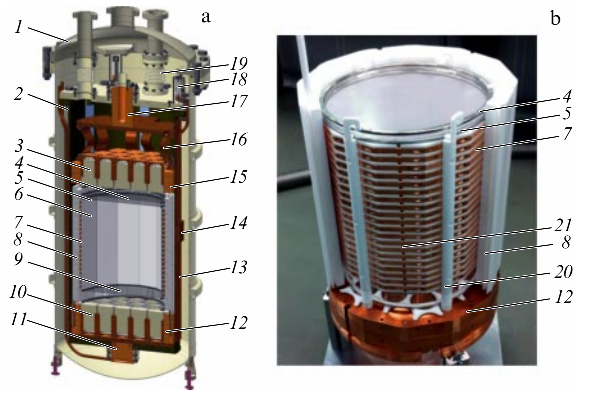

Figure 6. (a) Schematic cross section of the RED-100 detector and (b) a photograph of the inner elements of the detector during assembly: *1* — outer (warm) cryostat, *2* — inner (cold) cryostat, *3* — upper array of 19 Hamamatsu R11410-20 PMTs, *4* — mesh anode, *5* — mesh emission electrode, *6* — Teflon reflector, *7* — field-shaping rings, *8* — Teflon displacers, *9* — mesh cathode, *10* — bottom array of 19 PMTs, *11* — bottom thermosyphon cooler, *12* — copper housing of the bottom PMT array, *13* — copper cover of the cold cryostat, *14* — one of two side thermosyphon coolers, *15* — copper housing of the top PMT array, *16* — flexible thermal bridge, *17* — top thermosyphon cooler, *18* — thermal decoupling suspension, *19* — bellows-sealed thermal decoupling of pipelines, *20* — Teflon holders, and *21* — voltage-dividing resistor chain.

The planned location of the detector is beneath one of the power-generating units of WWER-1000 at the Kalinin NPP with the thermal power of 3 GW. One of the technical rooms beneath the reactor is located at 'zero' level (the ground level) and can be used to perform the experiment. The detector location is 19 m from the reactor core, and the neutrino flux at this point is 1.35×10^{13} cm^{-2} s^{-1}. The concrete roofing of the power-generating unit, the reactor itself, and the spent fuel storage pools located above provide quite significant shielding from the cosmic background with the overall thickness equivalent of approximately 60 m.w.e., which significantly exceeds the shielding thickness in foreign NPPs, where it is usually impossible to install the setups beneath the nuclear reactor.

With the lowest possible threshold of approximately 300 eV, which corresponds to two ionization electrons, the expected count rate of the detector in the FV of 100 kg should be around 3300 counts per day [86], which is two orders of magnitude higher than the count rate in germanium detector setups [43–45]. Modeling the detector has shown that the main source of the background are cosmic neutrons, which have quite a hard spectrum, reaching the energy range up to hundreds of MeV. Such neutrons elastically scatter on atomic nuclei at very small

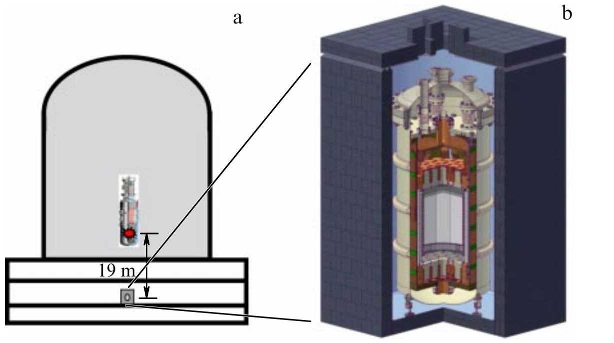

Figure 7. (a) Planned layout of the RED-100 detector at the Kalinin NPP and (b) the detector layout in the passive shielding (a lead layer approximately 10 cm in thickness and a 15 cm layer of water).

angles and produce recoil nuclei with keV and sub-keV energies. Figure 7 [86] shows a minimal version of the passive shielding (a 10 cm layer of lead and a 15 cm layer of water). Estimates show that with such shielding, the neutron background and the neutrino signal have the same order of magnitude. Background conditions can be measured during reactor shutdown (about 1 month) for refueling.

This means that the RED-100 detector will allow registering the CEνNS process with very high statistical accuracy. Simultaneously, other problems of neutrino physics can be worked on, such as the search for sterile neutrinos [87] (if it is possible to move the detector along the vertical by several meters) and a significant improvement in the bounds on the half-life of the neutrinoless and two-neutrino modes of the $2\beta^+$ and $K\beta^+$ decays of the ^{124}Xe and ^{78}Kr isotopes [88, 89]. The last isotope can be added to xenon in the amount of about 100 g, which does not significantly affect the detector characteristics.

The next stage of the experiment could be the scaling up of the RED-100 detector by 10 times and reaching the fiducial mass of 1 ton [90]. We note that the transition to the 1 ton scale is not a fantasy: such detectors are already used in experiments on the search for dark matter [91, 92] and there are ongoing developments in detectors with a liquid-xenon mass of more than several tons [93, 94]. The count rate of such a 1 ton detector would be an order of magnitude higher, around 0.5 Hz, and the detector would therefore ‘count’ neutrinos almost like a Geiger counter, while the radiation background would be significantly lower due to the self-shielding. For data collection over 10 days, such a count rate should provide a statistical accuracy that would be enough to see a change in the neutrino flux over the same period due to the processes considered in Section 4.1.

7. Conclusions

The process of coherent elastic neutrino–nucleus scattering predicted more than 40 years ago has finally been observed experimentally. This was done at the SNS proton accelerator of the Oak Ridge National Laboratory by the COHERENT international collaboration, which includes the authors of this paper. The experimental data is obtained at the setup based on a CsI[Na] scintillation crystal located at a distance of 20 m from the accelerator target, which is a strong source of three types of neutrinos: muon neutrinos and antineutrinos, and electron neutrinos.

After the first experimental confirmation of this process, interest was generated in studying it using detectors with other elemental compositions: with other numbers of nucleons in the atomic nuclei and in other energy ranges. The next significant step would be a CEνNS observation of the electron antineutrino emitted by the nuclear reactor of a power plant. Such an experiment would allow obtaining the process cross section using a ‘pure’ antineutrino flux. The current development of the detecting technology for reactor antineutrinos makes such an experiment possible and opens new opportunities for the development of systems for nonintrusive neutrino monitoring of nuclear objects. Our team is currently developing the two-phase liquid-xenon emission detector RED-100, which has a record high working medium mass and a threshold of less than 0.5 keV, which provides it with a record high sensitivity to this process.

This work was supported by the Russian Science Foundation (contract no. 18-12-00135, 12.04.18) and by the Academic Excellence Project of the National Research Nuclear University (NRNU) MEPhI (contract 02.a03.21.0005). The work on the analysis of the data from the CsI and CENNS-10 detectors was supported by the Russian Foundation for Basic Research grant no. 17-02-01077_a. The RED-100 detector was assembled with financial support from the governmental contract between NRNU MEPhI and the Ministry of Science and Higher Education of the Russian Federation 11.G34.31.0049 from October 19 2011 in the framework of the Russian Federation Government grant 220. The authors are members of the COHERENT international scientific collaboration and are deeply grateful to all other participants. The authors thank M I Vysotsky (Alikhanov Institute of Theoretical and Experimental Physics of the National Research Center ‘Kurchatov Institute’) for the fruitful discussions.

References

1. Kudenko Yu G *Phys. Usp.* **57** 462 (2014); *Usp. Fiz. Nauk* **184** 502 (2014)
2. Barabash A S *Phys. Usp.* **57** 482 (2014); *Usp. Fiz. Nauk* **184** 524 (2014)
3. Bilenky S M *Phys. Usp.* **57** 489 (2014); *Usp. Fiz. Nauk* **184** 531 (2014);
4. Olshevskiy A G *Phys. Usp.* **57** 497 (2014); *Usp. Fiz. Nauk* **184** 539 (2014)
5. Gorbunov D S *Phys. Usp.* **57** 503 (2014); *Usp. Fiz. Nauk* **184** 545 (2014)
6. Derbin A V *Phys. Usp.* **57** 512 (2014); *Usp. Fiz. Nauk* **184** 555 (2014)
7. Bednyakov V A, Naumov D V, Smirnov O Yu *Phys. Usp.* **59** 225 (2016); *Usp. Fiz. Nauk* **186** 233 (2016)
8. Akimov D et al. *Science* **357** 1123 (2017)
9. Kopeliovich V B, Frankfurt L L *JETP Lett.* **19** 145 (1974); *Pis'ma Zh. Eksp. Teor. Fiz.* **19** 236 (1974)
10. Freedman D Z *Phys. Rev. D* **9** 1389 (1974)
11. Hasert F J et al. *Phys. Lett. B* **46** 138 (1973)
12. Freedman D Z, Schramm D N, Tubbs D L *Annu. Rev. Nucl. Sci.* **27** 167 (1977)
13. Beacom J F, Farr W M, Vogel P *Phys. Rev. D* **66** 033001 (2002)
14. Barranco J, Miranda O G, Rashba T I *JHEP* **2005** (12) 021 (2005)
15. Drukier A, Stodolsky L *Phys. Rev. D* **30** 2295 (1984)
16. Barranco J, Miranda O G, Rashba T I *Phys. Rev. D* **76** 073008 (2007)
17. Dutta B et al. *Phys. Rev. D* **93** 013015 (2016)
18. Liao J, Marfatia D *Phys. Lett. B* **775** 54 (2017)
19. Eidelman S et al. (Particle Data Group) *Phys. Lett. B* **592** 1 (2004)
20. Bennett G W et al. (Muon g-2 Collab.) *Phys. Rev. D* **73** 072003 (2006)
21. Jegerlehner F, Nyffeler A *Phys. Rep.* **477** 1 (2009)

22. Fujikawa K, Shrock R E *Phys. Rev. Lett.* **45** 963 (1980)
23. Cañas B C et al. *Phys. Lett. B* **753** 191 (2016)
24. Beda A G et al. *Adv. High Energy Phys.* **2012** 350150 (2012)
25. Kosmas T S et al. *Phys. Rev. D* **92** 013011 (2015)
26. Auerbach L B et al. (LSND Collab.) *Phys. Rev. D* **63** 112001 (2001)
27. Amanik P S, McLaughlin G C *J. Phys. G* **36** 015105 (2009)
28. Patton K et al. *Phys. Rev. C* **86** 024612 (2012)
29. Cadeddu M et al. *Phys. Rev. Lett.* **120** 072501 (2018)
30. Ardellier F et al., hep-ex/0405032
31. Mikaelyan L A, in *Proc. of the Intern. Conf. on Neutrino Physics and Neutrino Astrophysics Neutrino-77, 18 – 24 June 1977, Baksan Valley* Vol. 2 (Moscow: Nauka, 1978) p. 383
32. Klimov Yu V et al. *Atom. Energy* **76** 123 (1994); *Atom. Energ.* **76** 130 (1994)
33. ν-SNS Collab., Proposal for a Neutrino Facility at the Spallation Neutron Source (Oak Ridge, Tenn.: Physics Division of the Oak Ridge National Laboratory, 2005); http://www.phy.ornl.gov/nusns/proposal.pdf
34. Scholberg K *J. Phys. Conf. Ser.* **606** 012010 (2015)
35. Goodman M W, Witten E *Phys. Rev. D* **31** 3059 (1985)
36. Collar J I, Giomataris Y *Nucl. Instrum. Meth. Phys. Res. A* **471** 254 (2001)
37. Barbeau P S et al. *IEEE Trans. Nucl. Sci.* **50** 1285 (2003)
38. Kopylov A V et al. *Adv. High Energy Phys.* **2014** 147046 (2014)
39. Barbeau P S, Collar J I, Tench O *JCAP* **2007** (09) 009 (2007)
40. Cabrera-Palmer B, Reyna D ''Development of Coherent Germanium Neutrino Technology (CoGeNT) for Reactor Safeguards'', Sandia Report SAND2012-8021 (Albuquerque, N.Mex., Livermore, Califo.: Sandia National Laboratories, 2012)
41. Wong H T *Nucl. Phys. B Proc. Suppl.* **138** 333 (2005)
42. Soma A K et al. *Nucl. Instrum. Meth. Phys. Res. A* **836** 67 (2016)
43. Belov V et al. *JINST* **10** P12011 (2015)
44. Medvedev D ''Investigation of neutrino properties with Ge detectors on KNPP'', in *Intern. Session–Conf. of the Section of Nuclear Physics of the Physical Sciences Department of the Russian Academy of Sciences ''Physics of Fundamental Interactions'' Dedicated to 50th Anniversary of Baksan Neutrino Observatory, Nalchik, Russian Federation, June 6 – 8, 2017*
45. Buck C et al. ''The CONUS Experiment – COherent elastic NeUtrino nucleus Scattering'', in *15th Intern. Conf. on Topics in Astroparticle and Underground Physics, TAUP2017, Sudbury, Canada, July 24 – 28, 2017*
46. Billard J et al. *J. Phys. G* **44** 105101 (2017)
47. Abe Y et al. (Double Chooz Collab.) *Phys. Rev. Lett.* **108** 131801 (2012)
48. Formaggio J A ''Using low temperature bolometers for coherent neutrino scattering'', in *Workshop on Table-Top Experiments with Skyscraper Reach, Cambridge, Mass., USA, August 9 – 11, 2017*
49. Leder A et al. *JINST* **13** P02004 (2018)
50. The MINER Experiment, http://miner.physics.tamu.edu/index.html#
51. Agnolet G et al. *Nucl. Instrum. Meth. Phys. Res. A* **853** 53 (2017)
52. Chapellier M P *J. Low Temp. Phys.* **178** 237 (2015)
53. Strauss R et al. *Eur. Phys. J. C* **77** 506 (2017)
54. Aguilar-Arevalo A et al. *J. Phys. Conf. Ser.* **761** 012057 (2016)
55. Bolozdynya A et al. *IEEE Trans. Nucl. Sci.* **42** 565 (1995)
56. Dolgoshein B A, Lebedenko V N, Rodionov B U *JETP Lett.* **11** 351 (1970); *Pis'ma Zh. Eksp. Teor. Fiz.* **11** 513 (1970)
57. Hagmann C, Bernstein A *IEEE Trans. Nucl. Sci.* **51** 2151 (2004)
58. Sangiorgio S et al. *Phys. Proc.* **37** 1266 (2012)
59. Joshi T H et al. *Phys. Rev. Lett.* **112** 171303 (2014)
60. Sangiorgio S et al. *Nucl. Instrum. Meth. Phys. Res. A* **728** 69 (2013)
61. Bondar A et al. *JINST* **12** C05016 (2017)
62. Hitachi A et al. *Phys. Rev. B* **27** 5279 (1983)
63. Wahl C G et al. *JINST* **9** P06013 (2014)
64. Akimov D et al. *J. Phys. Conf. Ser.* **798** 012210 (2017)
65. Scholberg K et al., arXiv:0910.1989
66. Akimov D et al., arXiv:1803.09183
67. Brice S J et al. *Phys. Rev. D* **89** 072004 (2014)
68. Edwards B et al. *Astropart. Phys.* **30** 54 (2008)
69. Burenkov A A et al. *Phys. Atom. Nucl.* **72** 653 (2009); *Yad. Fiz.* **72** 693 (2009)
70. Akimov D et al. *JINST* **4** P06010 (2009)
71. Santos E et al. (ZEPLIN-III Collab.) *J. High Energ. Phys.* **2011** 115 (2011)
72. Sorensen P et al. (XENON10 Collab.) *Nucl. Instrum. Meth. Phys. Res. A* **601** 339 (2009)
73. Thomas J, Imel D A *Phys. Rev. A* **36** 614 (1987)
74. Szydagis M et al. *JINST* **6** P10002 (2011)
75. NEST. Noble Element Simulation Technique. UC Davis, Department of Physics, http://nest.physics.ucdavis.edu/site/
76. Akimov D et al. (COHERENT Collab.), arXiv:1509.08702
77. Collar J I et al. *Nucl. Instrum. Meth. Phys. Res. A* **773** 56 (2015)
78. Konovalov A ''Observation of CEvNS at SNS'', in *18th Lomonosov Conf. on Elementary Particle Physics, Moscow, Russian Federation, August 24 – 30, 2017*
79. Efremenko Yu ''First Observation of Coherent Elastic Neutrino-Nucleus Scattering (CEvNS)'', in *νEclipse 2017 Workshop: New Extensions of Coherent Scattering and other Lepton Interactions for New Physics Searches, Knoxville, Tenn., USA, August 20 – 22, 2017*
80. Bhatia C et al. *Nucl. Instrum. Meth. Phys. Res. A* **757** 7 (2014)
81. Brice S J et al. *Phys. Rev. D* **89** 072004 (2014)
82. Mascarenhas N et al. *IEEE Trans. Nucl. Sci.* **56** 1269 (2009)
83. Pozzi S A et al. *Nucl. Instrum. Meth. Phys. Res. A* **694** 119 (2012)
84. Lazauskas R, Volpe C *J. Phys. G* **37** 125101 (2010)
85. Lazauskas R, Volpe C *J. Phys. G* **42** 059501 (2015)
86. Akimov D Yu et al. *JINST* **12** C06018 (2017)
87. Cañas B C et al. *Phys. Lett. B* **776** 451 (2018)
88. Bolozdynya A et al. *IEEE Trans. Nucl. Sci.* **44** 1046 (1997)
89. Bolozdynya A ''Emission two-phase xenon detector RED-100 to search for coherent neutrino elastic scattering off xenon nuclei'', in *Intern. Session–Conf. of the Section of Nuclear Physics of the Physical Sciences Department of the Russian Academy of Sciences ''Physics of Fundamental Interactions'' Dedicated to 50th Anniversary of Baksan Neutrino Observatory, Nalchik, Russian Federation, June 6 – 8, 2017*
90. Akimov D ''The RED-100 experiment'', in *The 2nd Intern. Conf. on Particle Physics and Astrophysics, ICPPA 2016, Moscow, Russian Federation, October 10 – 14, 2016*
91. Cui X et al. (PandaX-II Collab.) *Phys. Rev. Lett.* **119** 181302 (2017)
92. Aprile E et al. (XENON Collab.) *Phys. Rev. Lett.* **119** 181301 (2017)
93. Aprile E et al. *JCAP* **2016** (04) 027 (2016)
94. Mount B J et al. (LZ Collab.), LBNL-1007256; arXiv:1703.09144